3. Interaction Mechanisms

The variety of interaction mechanisms that may occur when applying laser light to biological tissue is manifold. Specific tissue characteristics as well as laser parameters contribute to this diversity. Most important among optical tissue properties are the coefficients of reflection, absorption, and scattering which were discussed in detail in the preceding chapter. Together, they determine the total transmission of the tissue at a certain wavelength. Thermal tissue properties – such as heat conduction and heat capacity – will be added in this chapter. On the other hand, the following parameters are given by the laser radiation itself: wavelength, exposure time, applied energy, focal spot size, energy density, and power density[1]. Among these, the exposure time is a very crucial parameter when selecting a certain type of interaction, as we will find later on.

During the first decades after the invention of the laser by Maiman (1960), many studies were conducted investigating potential interaction effects by using all types of laser systems and tissue targets. Although the number of possible combinations for the experimental parameters is unlimited, mainly five categories of interaction types are classified today. These are *photochemical interactions*, *thermal interactions*, *photoablation*, *plasma-induced ablation*, and *photodisruption*. Each of these interaction mechanisms will be thoroughly discussed in this chapter. In particular, the physical principles governing these interactions are reviewed. Emphasis is placed on microscopic mechanisms controlling various processes of laser energy conversion. Each type of interaction will be introduced by common macroscopic observations including typical experimental data and/or histology of tissue samples after laser exposure. At the end of each discussion, a comprehensive summary of the specific interaction mechanism is given.

Before going into detail, an interesting result shall be stated. All these seemingly different interaction types share a single common datum: the characteristic energy density ranges from approximately $1\,\mathrm{J/cm^2}$ to $1000\,\mathrm{J/cm^2}$.

[1] In the literature, the terms used for radiometric parameters such as fluence, irradiance, intensity, and energy dose are often somewhat confusing. Throughout this book, the following agreements are met: *power* is expressed in units of W, *energy* in units of J, the synonyms *power density*, *intensity*, and *irradiance* in units of $\mathrm{W/cm^2}$, the synonyms *energy density*, *fluence*, and *radiant exposure* in units of $\mathrm{J/cm^2}$, and *energy dose* in units of $\mathrm{J/cm^3}$ (see also the Appendix).

This is surprising, since the power density itself varies over 15 orders of magnitude! Thus, a single parameter distinguishes and primarily controls these processes: the duration of laser exposure which is mainly identical with the interaction time itself.

A double-logarithmic map with the five basic interaction types is shown in Fig. 3.1 as found in several experiments. The ordinate expresses the applied power density or irradiance in W/cm^2. The abscissa represents the exposure time in seconds. Two diagonals show constant energy fluences at $1\,J/cm^2$ and $1000\,J/cm^2$, respectively. According to this chart, the time scale can be roughly divided into five sections: continuous wave or exposure times $> 1\,s$ for *photochemical interactions*, 1 min down to 1 µs for *thermal interactions*, 1 µs down to 1 ns for *photoablation*, and $< 1\,ns$ for *plasma-induced ablation* and *photodisruption*. The difference between the latter two is attributed to different energy densities. They will be addressed separately in Sects. 3.4 and 3.5, since one of them is solely based on ionization, whereas the other is an associated but primarily mechanical effect.

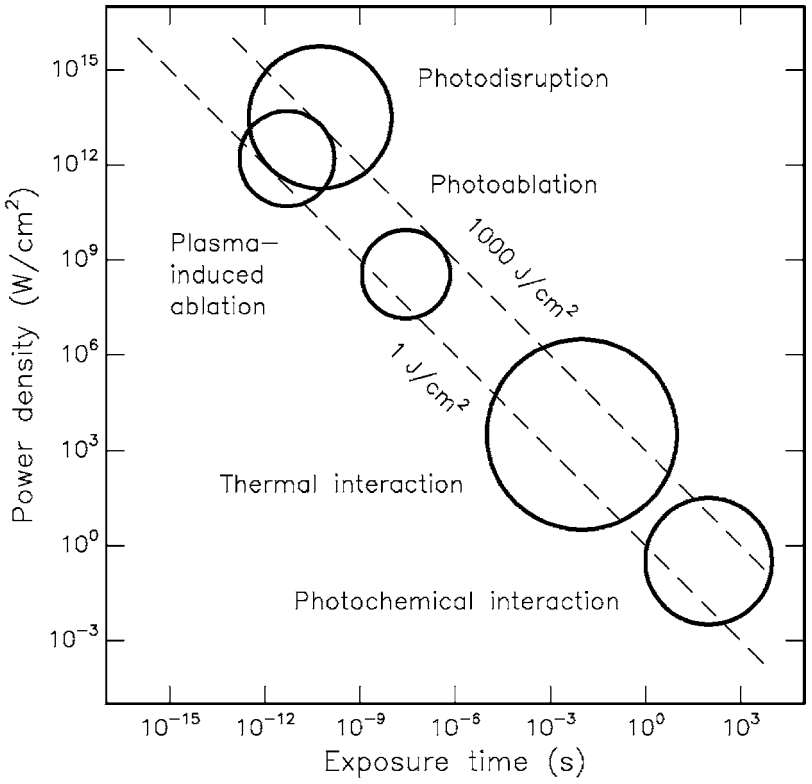

Fig. 3.1. Map of laser–tissue interactions. The circles give only a rough estimate of the associated laser parameters. Modified from Boulnois (1986)

Obviously, Fig. 3.1 proves the statement from above that the total energy density relevant for medical laser applications ranges from about $1\,\mathrm{J/cm^2}$ to $1000\,\mathrm{J/cm^2}$. The reciprocal correlation between power density and exposure time clearly demonstrates that roughly the same energy density is required for any intended type of interaction. Thus, the exposure time appears to be the main parameter responsible for the variety of interaction mechanisms.

Adjacent interaction types cannot always be strictly separated. As shown in the following sections, thermal effects may also play an important role during photochemical interaction. And even ultrashort laser pulses with pulse durations shorter than 100 ps – each of them having no thermal effect – may add up to a measurable increase in temperature if applied at repetition rates higher than about 10–20 Hz, depending on the laser. These two examples reveal our need for a better understanding of each laser–tissue interaction. This task, of course, is aggravated due to the inhomogeneity of most tissues which cannot be altered. However, the basic physics involved in each interaction becomes accessible if enough data are collected to fit unknown parameters.

3.1 Photochemical Interaction

The group of photochemical interactions stems from empirical observations that light can induce chemical effects and reactions within macromolecules or tissues. One of the most popular examples was created by evolution itself: the energy release due to photosynthesis. In the field of medical laser physics, photochemical interaction mechanisms play a significant role during *photodynamic therapy (PDT)*. Frequently, *biostimulation* is also attributed to photochemical interactions, although this is not scientifically ascertained. After a detailed description of the physical background, both of these methods will be discussed in this section.

Photochemical interactions take place at very low power densities (typically $1\,\mathrm{W/cm^2}$) and long exposure times ranging from seconds to continuous wave. Careful selection of laser parameters yields a radiation distribution inside the tissue that is determined by scattering. In most cases, wavelengths in the visible range (e.g. Rhodamine dye lasers at 630 nm) are used because of their efficiency and their high optical penetration depths. The latter are of importance if deeper tissue structures are to be reached.

During PDT, spectrally adapted chromophores are injected into the body. Monochromatic irradiation may then trigger selective photochemical reactions, resulting in certain biological transformations. A chromophore compound which is capable of causing light-induced reactions in other nonabsorbing molecules is called a *photosensitizer*. After resonant excitation by laser irradiation, the photosensitizer performs several simultaneous or sequential decays which result in intramolecular transfer reactions. At the end of these diverse reaction channels, highly cytotoxic reactands are released causing an irreversible oxidation of essential cell structures. Thus, the main

idea of photochemical treatment is to use a chromophore receptor acting as a catalyst. Its excited states are able to store energy transferred from resonant absorption, and their deactivation leads to toxic compounds leaving the photosensitizer in its original state. Therefore, this type of interaction is also called *photosensitized oxidation*.

Most photosensitizers belong to the group of organic dyes. Their electronic states are characterized by singlet states (total electron spin momentum $s=0$) and triplet states ($s=1$). Furthermore, each electronic state is subdivided into a band of vibrational states. Intersystem crossing is permitted but is associated with an increased lifetime.

Potential reaction kinetics of the photosensitizer are listed in Table 3.1. The reaction types can be characterized by either *excitation*, *decays*, *Type I* or *Type II reactions*, and *carotenoid protection*.

Table 3.1. Kinetics of photosensitization (S: photosensitizer, RH: substrate with H-bond, CAR: carotenoid). Modified from Boulnois (1986)

Excitation	
• Singlet state absorption	$^1\mathrm{S} + h\nu \Longrightarrow {}^1\mathrm{S}^*$
Decays	
• Radiative singlet decay	$^1\mathrm{S}^* \Longrightarrow {}^1\mathrm{S} + h\nu'$ (*fluorescence*)
• Nonradiative singlet decay	$^1\mathrm{S}^* \Longrightarrow {}^1\mathrm{S}$
• Intersystem crossing	$^1\mathrm{S}^* \Longrightarrow {}^3\mathrm{S}^*$
• Radiative triplet decay	$^3\mathrm{S}^* \Longrightarrow {}^1\mathrm{S} + h\nu''$ (*phosphorescence*)
• Nonradiative triplet decay	$^3\mathrm{S}^* \Longrightarrow {}^1\mathrm{S}$
Type I reactions	
• Hydrogen transfer	$^3\mathrm{S}^* + \mathrm{RH} \Longrightarrow \mathrm{SH}^\bullet + \mathrm{R}^\bullet$
• Electron transfer	$^3\mathrm{S}^* + \mathrm{RH} \Longrightarrow \mathrm{S}^{\bullet -} + \mathrm{RH}^{\bullet +}$
• Formation of hydrogen dioxide	$\mathrm{SH}^\bullet + {}^3\mathrm{O}_2 \Longrightarrow {}^1\mathrm{S} + \mathrm{HO}_2^\bullet$
• Formation of superoxide anion	$\mathrm{S}^{\bullet -} + {}^3\mathrm{O}_2 \Longrightarrow {}^1\mathrm{S} + \mathrm{O}_2^\bullet$
Type II reactions	
• Intramolecular exchange	$^3\mathrm{S}^* + {}^3\mathrm{O}_2 \Longrightarrow {}^1\mathrm{S} + {}^1\mathrm{O}_2^*$
• Cellular oxidation	$^1\mathrm{O}_2^* + \mathrm{cell} \Longrightarrow \mathrm{cell}_{\mathrm{ox}}$
Carotenoid protection	
• Singlet oxygen extinction	$^1\mathrm{O}_2^* + {}^1\mathrm{CAR} \Longrightarrow {}^3\mathrm{O}_2 + {}^3\mathrm{CAR}^*$
• Deactivation	$^3\mathrm{CAR}^* \Longrightarrow {}^1\mathrm{CAR} + \mathrm{heat}$

After the absorption of laser photons, the photosensitizer is first transferred to an excited singlet state $^1\mathrm{S}^*$. Then, three potential decay channels are available: nonradiative and radiative singlet decay to the singlet ground state, and intersystem crossing to an excited triplet state. The latter, finally, may also promote to the singlet ground state by either nonradiative

or radiative triplet decay. The radiative singlet and triplet decays are called *fluorescence* and *phosphorescence*, respectively. Typical lifetimes of fluorescence are of the order of nanoseconds, whereas phosphorescence may last up to a few milliseconds or seconds. According to Foote (1968), two alternative reaction mechanisms exist for the decay of the excited triplet state which are called *Type I* and *Type II* reactions (see Table 3.1). They are characterized by either the generation of free radicals (Type I) or the transfer of excitation energy to oxygen molecules (Type II).

During Type I reactions, the triplet state next interacts with a target molecule, other than oxygen, resulting in the release of free neutral or ionized radicals. Further reaction with triplet oxygen may lead to the formation of hydrogen dioxide or superoxide anions. In Type II reactions, the triplet state of the photosensitizer directly interacts with molecular triplet oxygen $^3O_2$ which is then transferred to an excited singlet state $^1O_2^*$. During this reaction, the electronic spins are flipped in the following manner:

$$\overset{\uparrow\uparrow}{{}^3S^*} + \overset{\uparrow\uparrow}{{}^3O_2} \Longrightarrow \overset{\uparrow\downarrow}{{}^1S} + \overset{\uparrow\downarrow}{{}^1O_2^*}\,.$$

Excited singlet oxygen $^1O_2^*$ is very reactive, thus leading to cellular oxidation and necrosis. For instance, Weishaupt et al. (1986) identified singlet oxygen as the toxic agent in photoactivation of tumor cells. To avoid additional oxidation of healthy cells, carotin is injected after laser exposure which then promotes the toxic singlet oxygen to harmless triplet oxygen. Usually, Type I and Type II reactions take place at the same time. Which mechanism is favored mainly depends on the concentration of available triplet oxygen and appropriate target molecules.

3.1.1 Photodynamic Therapy (PDT)

Since the beginning of the 20th century, certain dyes have been known to induce photosensitizing effects as reported by von Tappeiner (1900). The first intended therapeutic application of dyes in combination with light was proposed by von Tappeiner and Jesionek (1903). Later, it was observed by Auler and Banzer (1942) that certain porphyrins have a long clearance period in tumor cells. If these dyes could somehow be transferred to a toxic state, e.g. by laser light, tumor cells could be preferentially treated. Kelly and Snell (1976) have reported on the first endoscopic application of a photosensitizer in the case of human bladder carcinoma. Today, the idea of photodynamic therapy has become one of the major pillars in the modern treatment of cancer.

Photodynamic therapy is performed as follows: first, a photosensitizer, e.g. hematoporphyrin derivative (HpD), is injected into a vein of the patient. In the case of HpD, 2.5–5 mg per kg body weight are applied. Within the next few hours, HpD is distributed among all soft tissues except the brain. The basic characteristic of a photosensitizer is that it remains inactive until irradiated. After 48–72 hours, most of it is cleared from healthy tissue. However,

its concentration in tumor cells has not decreased much even after a period of 7–10 days. Thus, HpD does not accumulate in tumor cells immediately after injection, but these cells show a longer storage ability (*affinity*) for HpD. The initial concentration is the same as in healthy cells, but the clearance is faster in the latter cells. After about three days, the concentration of HpD in tumor cells is about thirty times higher than in healthy cells.

Laser irradiation usually takes place after the third day and up to the seventh day after injection if several treatments are necessary. Within this period, tumor cells are still very sensitive and selective necrosis of tumor cells is enabled. However, many healthy tissues may retain certain constituents of HpD and are thus photosensitized, as well. Cellular effects of HpD were studied in detail by Moan and Christensen (1981) and Berns et al. (1982). The general procedure of photodynamic therapy is illustrated in Fig. 3.2.

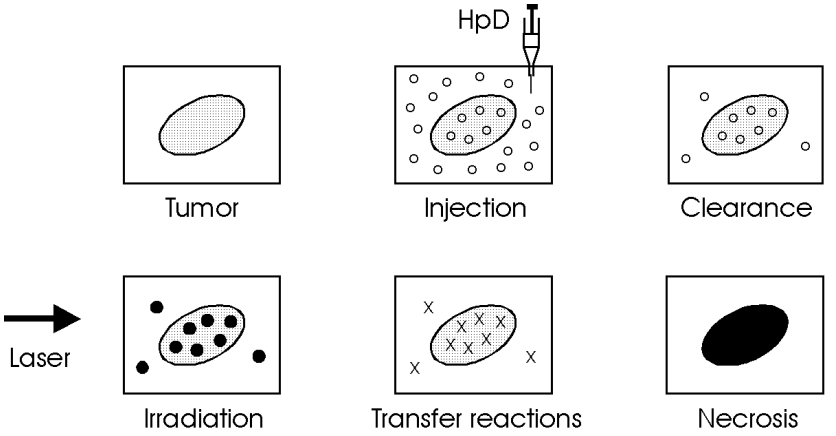

Fig. 3.2. Scheme of photodynamic therapy

Tumor treatment is the principal but not the only application field of photodynamic therapy. Malik et al. (1990) have observed bactericidal effects of laser-activated porphyrins. And recently, Wilson et al. (1993) have investigated the effect of different photosensitizers on *streptococcus sanguis*, a common bacterium of dental plaques. Some of their results are summarized in Figs. 3.3a–b. Obviously, only the combined action of photosensitizer and laser exposure significantly reduces the fraction of surviving bacteria.

One of the most commonly used photosensitizers in photodynamic therapy is a hematoporphyrin derivative called HpD. It is derived from calf blood and is a complex collection of different porphyrins, mainly

– dihematoporphyrin,
– hydroxyethylvinyl-deuteroporphyrin,
– protoporphyrin.

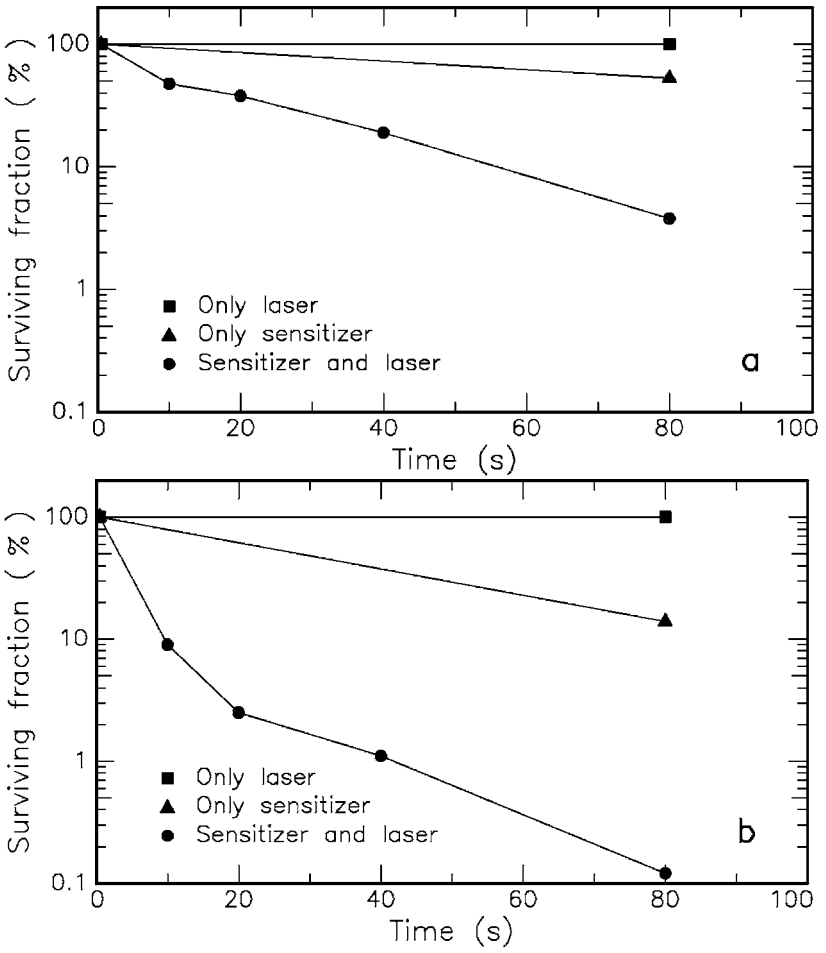

Fig. 3.3. (a) Effect of methylene blue and/or helium–neon laser (power: 7.3 mW) on the viability of streptococcus sanguis. **(b)** Effect of hematoporphyrin ester and/or helium–neon laser (power: 7.3 mW) on the viability of streptococcus sanguis. Data according to Wilson et al. (1993)

Among those substances, dihematoporphyrin is the active constituent in providing the photosensitizing effect. Medical application of HpD was first performed and reported by Lipson and Baldes (1961). Proprietary names for HpD include Photofrin I and Photofrin II. Both of these agents are complex chemical mixtures with the latter being enriched in the tumor-localizing fraction during PDT.

The chemical structure of dihematoporphyrin is shown in Fig. 3.4. It consists of two porphyrin rings connected by a C–O–C chain. According to Dolphin (1979), porphyrins are characterized by a high thermal stability and

a dark color (from Greek: $\pi o \rho \phi \upsilon \rho \alpha$ = purple). The absorption and fluorescence spectra of HpD are shown in Fig. 3.5, whereas Fig. 3.6 illustrates the corresponding energy level diagram. The strong absorption at 350–400 nm originates from the broad excitation band $^1S_2$ of the dye. The relative low absorption at approximately 620–630 nm is used for clinical purposes. At this wavelength, deeper structures can be reached compared to using UV light due to the lower absorption coefficient of most tissues in the red spectrum. Detailed studies on porphyrin photosensitizers are found in the book edited by Kessel and Dougherty (1983).

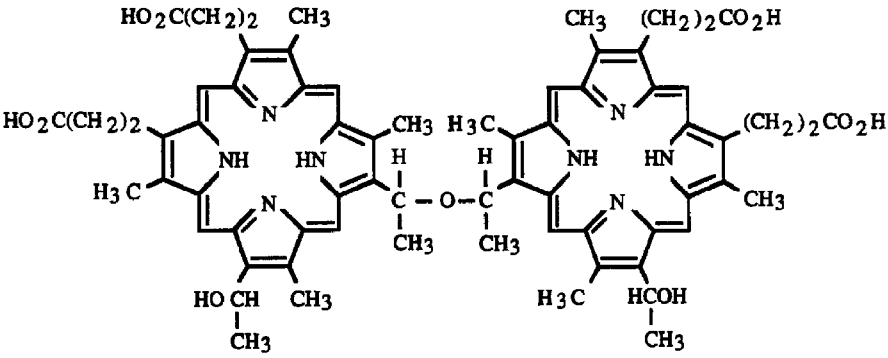

Fig. 3.4. Chemical structure of the active substance dihematoporphyrin which consists of two symmetric porphyrin rings

Primarily, the fluorescence spectrum of HpD is characterized by two peaks at 620 nm and 680 nm. They stem from the transitions $^1S_{1,0} \longrightarrow {}^1S_{0,0}$ and $^1S_{1,0} \longrightarrow {}^1S_{0,1}$, respectively. As in all macromolecules, the ground and the excited electronic states are further split into several vibrational states. After excitation, the macromolecule first relaxes to the lowest vibrational state belonging to the same excited electronic state. From there, it reaches the ground state by emitting fluorescence radiation.

The dependence of fluorescence on the concentration level of HpD is of considerable interest. It was found by Kinoshita (1988) that the emission peak at 620 nm decreases toward higher concentrations of HpD. This effect is explained by self-absorption which becomes a dominant process at concentrations higher than about 10^{-3} mol/l. Therefore, the comparison of relative fluorescence intensities is an indicator for the concentration level of HpD and, thus, for the distinction of tumor cells from healthy cells.

An even more powerful technique is given by *time-resolved fluorescence*. It was observed by Yamashita (1984) that the duration of the fluorescence decay of HpD also depends on its respective concentration level. The lowest investigated concentration of 8.4×10^{-6} mol/l yields a fluorescence decay time in the nanosecond range, whereas higher concentrations such as 8.4×10^{-3} mol/l are characterized by decays as short as a few hundred picoseconds. The time-

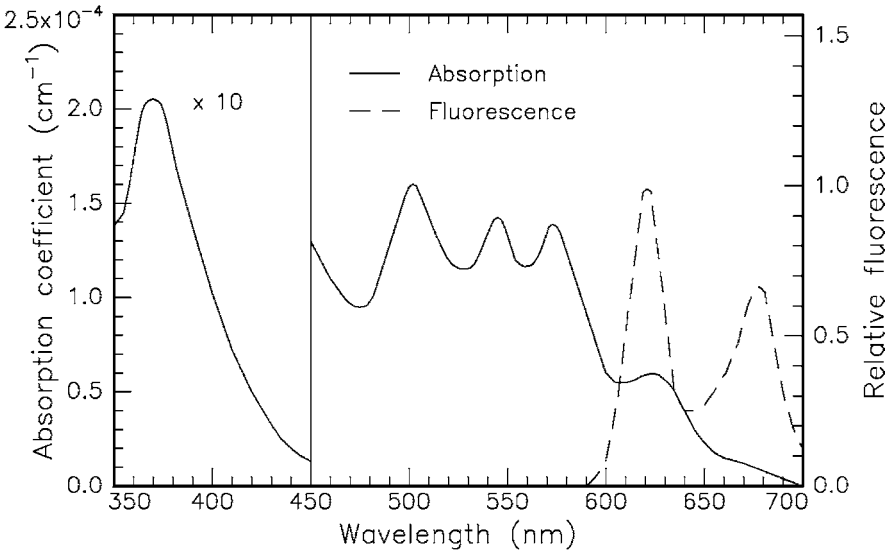

Fig. 3.5. Absorption and fluorescence spectra of hematoporphyrin derivative (HpD) dissolved in phosphate-buffered saline solution (PBS). Data according to Yamashita (1984)

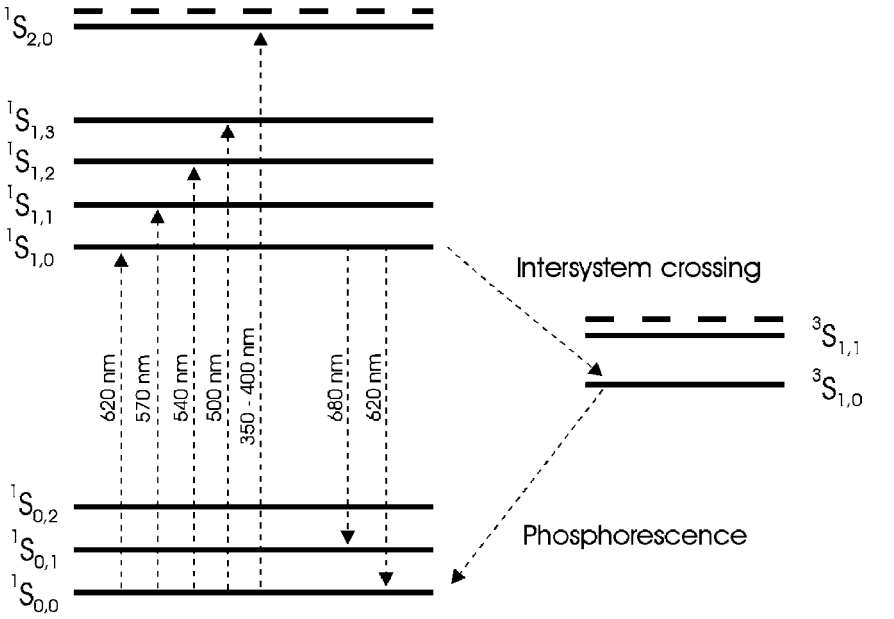

Fig. 3.6. Energy level diagram of HpD. Singlet (^{1}S) and triplet (^{3}S) states are shown. Dashed lines indicate higher excited states

resolved fluoresecence signals are summarized in Fig. 3.7. Tumor diagnosis can thus be established by time-gated detection of the fluorescence. For instance, Fig. 3.8 illustrates the decay in fluorescence intensity of healthy cells with respect to tumor cells as found by Kinoshita (1988). Since clearance of HpD is faster in healthy cells, the corresponding decay duration is significantly longer than in tumor cells. According to Unsöld et al. (1987), the simultaneous diagnosis and therapy of tumors with photosensitizers is one of the key advantages of PDT. Extensive in vivo studies of time-resolved fluorescence have been performed by Schneckenburger et al. (1993).

Meanwhile, the results of several experiments and clinical applications have been collected. It was found that other photosensitizers might even be more useful than HpD. The major disadvantage of HpD is the fact that the patient needs to remain in a dark room during the first weeks of therapy. This is necessary, because HpD is distributed all over the body, and sun light or artificial light would kill healthy tissue cells, as well. According to Kessel (1987), the primary adverse reaction of photodynamic therapy relates to the photosensitization of skin. Other disadvantages of HpD are:

– since HpD absorbs very poorly in the red and near infrared spectrum, only tumors very close to the surface can be treated,
– its concentration gradient among tumor and healthy cells could be steeper,
– the production of HpD from calf blood is very expensive.

However, the initial isolation in the period between injection of HpD and laser irradiation remains and is one of the biggest problems for patients. This context also explains the injection of carotenoids immediately after laser irradiation. These agents act as a protection system on a molecular basis, because they reverse the production of singlet oxygen by means of a triplet carotenoid state (compare Table 3.1). The protective property of carotenoids has been successfully tested by Mathews-Roth (1982).

Currently, further photosensitive compounds of a so-called second generation are under investigation concerning their applicability for PDT. These are, for instance, certain groups of phthalocyanins, naphthalocyanins and phorbides (reduced porphyrins) as reported by Spikes (1986), Firey and Rodgers (1987), and Röder et al. (1990). Hopefully, a dye will soon be found that is more efficient than HpD and overcomes its major disadvantage, the need for carotenoid protection. One potential candidate is meso-tetra-hydroxyphenyl-chlorin (mTHPC), a chemically well-defined substance compared to HpD. In order to achieve a similar extent of tumor necrosis, it was reported by Gossner et al. (1994) that in the case of mTHPC only one fifth of the light energy is needed compared to HpD. Another interesting substance is 5-aminolaevulinic acid (ALA) which itself is not even a photosensitizer but a precursor of the endogeneous synthesis of porphyrins. According to Loh et al. (1993), it can be orally administered rather than being injected like most of the porphyrins.

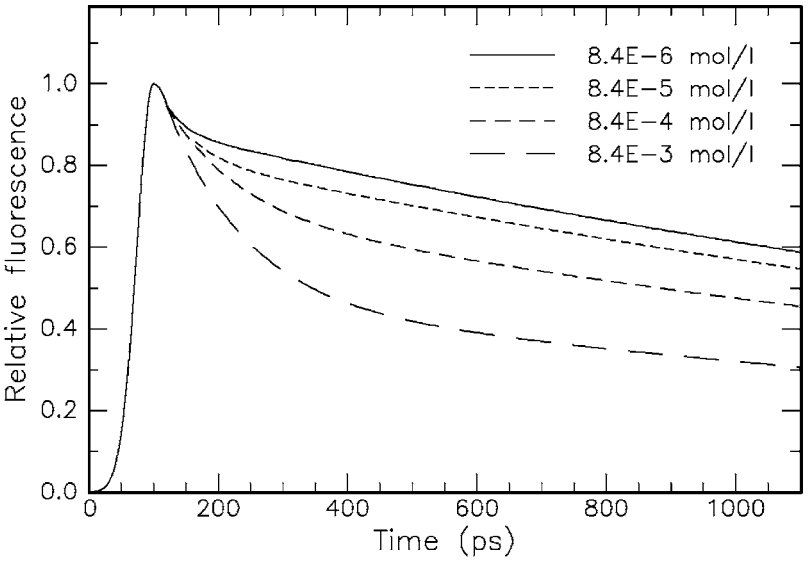

Fig. 3.7. Time-resolved fluorescence signals of HpD dissolved in phosphate-buffered saline solution (PBS). Concentrations of HpD as labeled. The corresponding decay durations of the fluorescence vary between approximately 350 ps and 2 ns. Data according to Yamashita (1984)

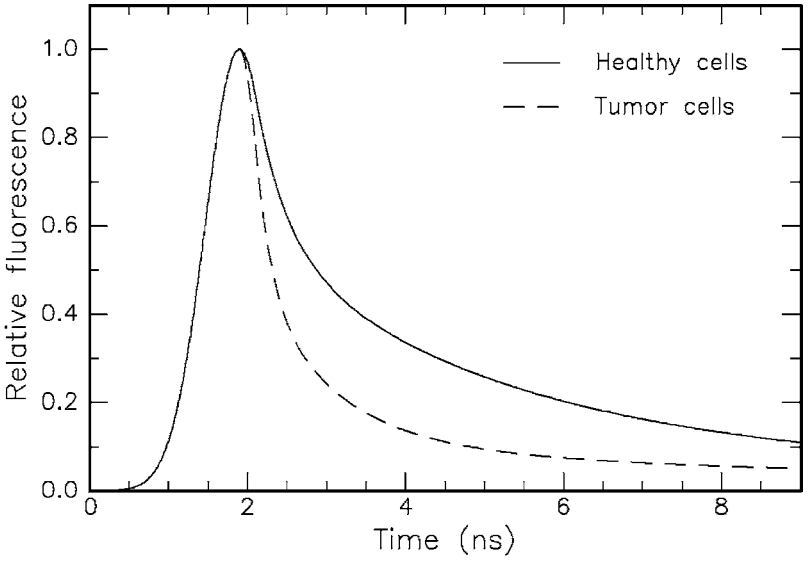

Fig. 3.8. Time-resolved HpD fluorescence of healthy cells versus tumor cells. The approximate decay durations are 2.5 ns and 1.0 ns, respectively. Data according to Kinoshita (1988)

Gossner et al. (1994) have compared the skin sensibility after application of DHE (dihematoporphyrin ester), mTHPC, and ALA. The results are graphically summarized in Fig. 3.9. The sensibility is measured in terms of a commonly used index of skin edema. It is interesting to observe that ALA induces least toxic skin damage. An increased sensibility is detectable only during the first two days after application. Although mTHPC is associated with the highest sensibility during the first week, only a slightly higher sensibility remains after the second week. This negative side effect during the first week is acceptable, though, since mTHPC is highly efficient in achieving tumor necrosis according to Gossner et al. (1994). The sensibility after application of DHE gradually decreases within the first four weeks and is still significantly enhanced at the end of this period. Thus, patients treated with DHE will have to remain in dark rooms for at least four weeks.

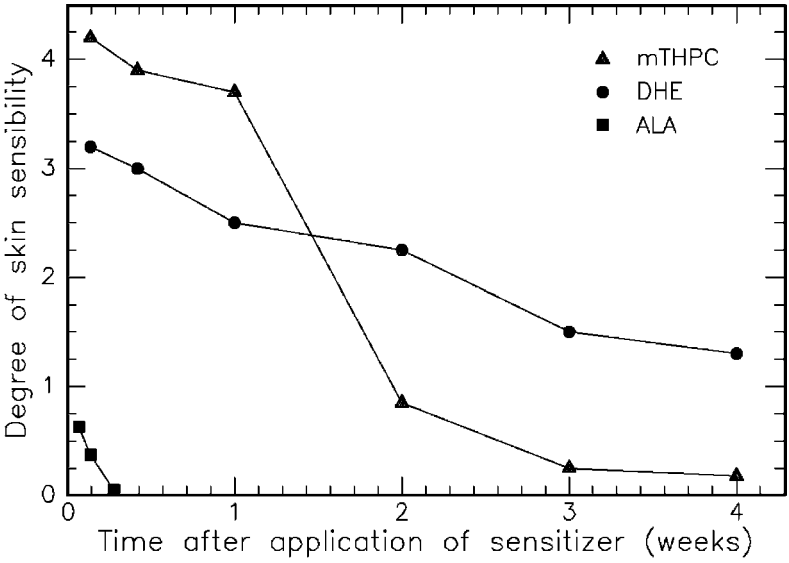

Fig. 3.9. Degree of skin sensibility after application of various photosensitizers as a function of time. Data according to Gossner et al. (1994)

The field of photodynamic tumor therapy has just begun to develop. Although much effort has already been made concerning treatment with HpD, a lot more research still needs to be done. Alternative photosensitizers such as mTHPC and ALA should be investigated in a large group of patients to further improve this type of treatment. Careful conclusions should then be drawn regarding their efficiency, indications, and potential contraindications. Finally, an approved committee has to compare all results with those obtained with other minimally invasive methods of tumor treatment such as exposure to ionizing radiation.

3.1.2 Biostimulation

Biostimulation is believed to occur at very low irradiances and to belong to the group of photochemical interactions. Unfortunately, the term *biostimulation* has not been scientifically very well defined, so far. The potential effects of extremely low laser powers (1–5 mW) on biological tissue have been a subject of controversy, since they were first claimed by the Hungarian surgeon Mester at the end of the 1960s. Wound healing and anti-inflammatory properties by red or near infrared light sources such as helium–neon lasers or diode lasers were reported. Typical energy fluences lie in the range 1–10 J/cm^2. In several cases, observers have noticed improvements for the patients. But in a few studies only, results could be verified by independent research groups. Moreover, contradictory results were obtained in many experiments.

The most significant studies concerning biostimulation are summarized in Table 3.2. They demonstrate the variety of potential application fields. However, often only very few patients were treated, and no clinical protocols were established. Furthermore, the success is rather doubtful, since in many of these diseases 50 % of the patients are spontaneously cured even without treatment. According to Wilder-Smith (1988), the distinction from an ordinary placebo effect is thus rather difficult to perform.

Table 3.2. Biostimulative effects investigated by different studies

Observation	Target	Laser type	Reference
Hair growth	Skin	Ruby	Mester et al. (1968)
Wound healing	Skin	Ruby	Mester et al. (1969)
			Mester et al. (1971)
		He-Ne	Brunner et al. (1984)
			Lyons et al. (1987)
No wound healing	Skin	He-Ne	Hunter et al. (1984)
			Strube et al. (1988)
		Argon ion	Jongsma et al. (1983)
			McCaughan et al. (1985)
Stimulated collagen synthesis	Fibroblasts	Nd:YAG	Castro et al. (1983)
		He-Ne	Kubasova et al. (1984)
			Boulton et al. (1986)
Suppressed collagen synthesis	Fibroblasts	Nd:YAG	Abergel et al. (1984)
Increased growth	Cells	Diode	Dyson and Young (1986)
Suppressed growth	Cells	He-Cd	Lin and Chan (1984)
		He-Ne	Quickenden et al. (1993)
Vascularization	Oral soft tissue	Diode	Kovacs et al. (1974)
			Cho and Cho (1986)
Pain relief	Teeth	He-Ne	Carrillo et al. (1990)
		Diode	Taube et al. (1990)
No pain relief	Teeth	He-Ne	Lundeberg et al. (1987)
		Diode	Roynesdal et al. (1993)

According to Karu (1987), local wound healing effects with helium–neon or diode lasers may be explained by the action of low-intensity light on cell proliferation. In the area of such injuries, conditions are usually created preventing proliferation such as low oxygen concentration or pH. The exposure to red or near infrared light might thus serve as a stimulus to increase cell proliferation. When irradiating fresh wounds, though, the effect of biostimulation is found to be minimal or even nonexistent. This observation is probably due to the fact that cell proliferation is very active in fresh wounds, and regeneration is not significantly altered by laser irradiation.

One remaining open question is, which of the characteristics of laser radiation – coherence, narrow bandwidth, polarization – is of primary importance for biostimulation? Or, in other words, does it necessarily have to be a laser or would an incoherent light source serve as well? Hence, biostimulation is still a research field with a lot of speculation involved. Usually, the controversy stems from our inability to specify the photochemical channels of potential reactions. Detailed investigations in this area and reproducible experimental results are badly needed.

3.1.3 Summary of Photochemical Interaction

- *Main idea:* using a photosensitizer acting as catalyst (only in photodynamic therapy)
- *Observations:* no macroscopic observations
- *Typical lasers:* red dye lasers, diode lasers
- *Typical pulse durations:* 1 s . . . CW
- *Typical power densities:* 0.01 . . . 50 $\mathrm{W/cm^2}$
- *Special applications:* photodynamic therapy, biostimulation

3.2 Thermal Interaction

The term *thermal interaction* stands for a large group of interaction types, where the increase in local temperature is the significant parameter change. Thermal effects can be induced by either CW or pulsed laser radiation. While photochemical processes are often governed by a specific reaction pathway, thermal effects generally tend to be nonspecific according to Parrish and Deutsch (1984). However, depending on the duration and peak value of the tissue temperature achieved, different effects like *coagulation*, *vaporization*, *carbonization*, and *melting* may be distinguished. In the following paragraphs, these effects shall first be visualized by selected photographs taken with either light microscopy or scanning electron microscopy (SEM). Afterwards, detailed models of heat generation, heat transport, and associated heat effects are given. Finally, the principles of laser-induced interstitial thermotherapy – a recently established treatment technique – are discussed.

Coagulation. The histologic appearance of coagulated tissue is illustrated in Figs. 3.10a–b. In one case, a sample of uterine tissue was coagulated using a CW Nd:YAG laser. In a histologic section, the coagulated area can be easily detected when staining the tissue with hematoxylin and eosin. Coagulated tissue appears significantly darker than other tissue. In the second photograph, 120 pulses from an Er:YAG laser were applied to an excised cornea. Again, the tissue was stained with hematoxylin and eosin. During the process of coagulation, temperatures reach at least 60°C, and coagulated tissue becomes necrotic as will be discussed in this section.

Vaporization. Another example of an important thermal effect is shown in Figs. 3.11a–b. A tooth was exposed to 20 pulses from an Er:YAG laser. During the ablation process, complete layers of tooth substance were removed leaving stair-like structures. This observation is attributed to the existence of so-called *striae of Retzius* which are layers with a high content of water molecules. Water strongly absorbs the Er:YAG wavelength at 2.94 µm as shown below, thus leading to vaporization within these layers. The induced increase in pressure – water tries to expand in volume as it vaporizes – leads to localized microexplosions with results as demonstrated in the enlargement in Fig. 3.11b. In the literature, vaporization is sometimes also referred to as a *thermomechanical effect* due to the pressure build-up involved. The resulting ablation is called *thermal decomposition* and must be distinguished from *photoablation* which will be described in Sect. 3.3.

Carbonization. In Fig. 3.12a, a sample of skin is shown which was exposed to a CW CO_2 laser for the purpose of treating metastases. In this case, however, too much energy was applied and carbonization occurred. Thus, the local temperature of the exposed tissue had been drastically increased. At temperatures above approximately 100°C, the tissue starts to carbonize, i.e. carbon is released, leading to a blackening in color. A similar effect is seen in Fig. 3.12b, where a tooth was exposed to a CW CO_2 laser. For medical laser applications, carbonization should be avoided in any case, since tissue already becomes necrotic at lower temperatures. Thus, carbonization only reduces visibility during surgery.

Melting. Finally, Figs. 3.13a–b show the surface of a tooth after exposure to 100 pulses from a Ho:YAG laser. In Fig. 3.13a, several cracks can be seen leaving the application spot radially. They originate from thermal stress induced by a local temperature gradient across the tooth surface. The edge of the interaction zone is shown in an enlargement in Fig. 3.13b. Melted and afterwards down-cooled tooth substance as well as gas bubbles are observed similar to solidified lava. The temperature must have reached a few hundred degrees Celsius to melt the tooth substance which mainly consists of hydroxyapatite, a chemical compound of calcium and phosphate as will be discussed in Sect. 4.2. Obviously, the pulse duration of a few microseconds is still long enough to enable a sufficient increase in temperature, since the applied repetition rate of 1 Hz is extremely low.

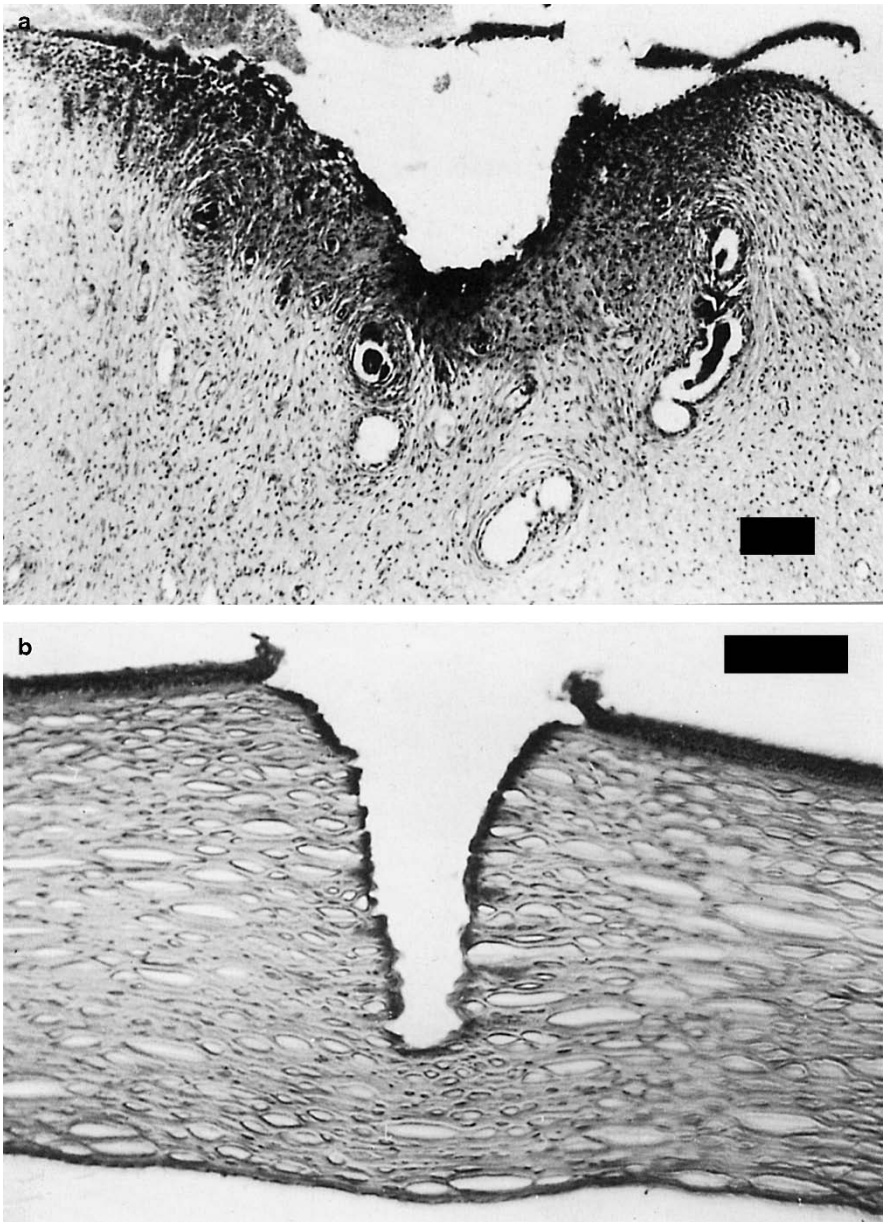

Fig. 3.10. (a) Uterine tissue of a wistar rat coagulated with a CW Nd:YAG laser (power: 10 W, bar: 80 µm). Photograph kindly provided by Dr. Kurek (Heidelberg). **(b)** Human cornea coagulated with 120 pulses from an Er:YAG laser (pulse duration: 90 µs, pulse energy: 5 mJ, repetition rate: 1 Hz, bar: 100 µm)

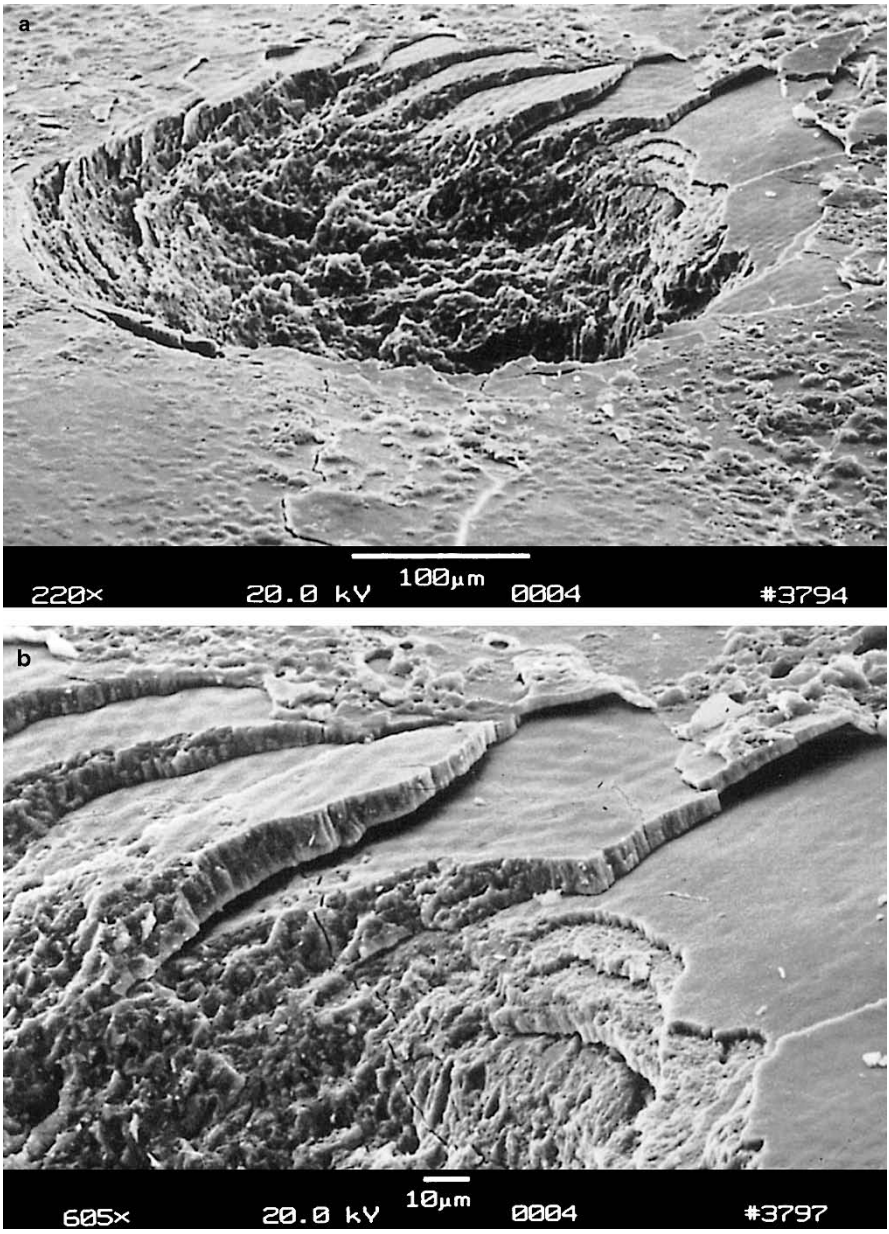

Fig. 3.11. (a) Human tooth vaporized with 20 pulses from an Er:YAG laser (pulse duration: 90 µs, pulse energy: 100 mJ, repetition rate: 1 Hz). **(b)** Enlargement showing the edge of ablation

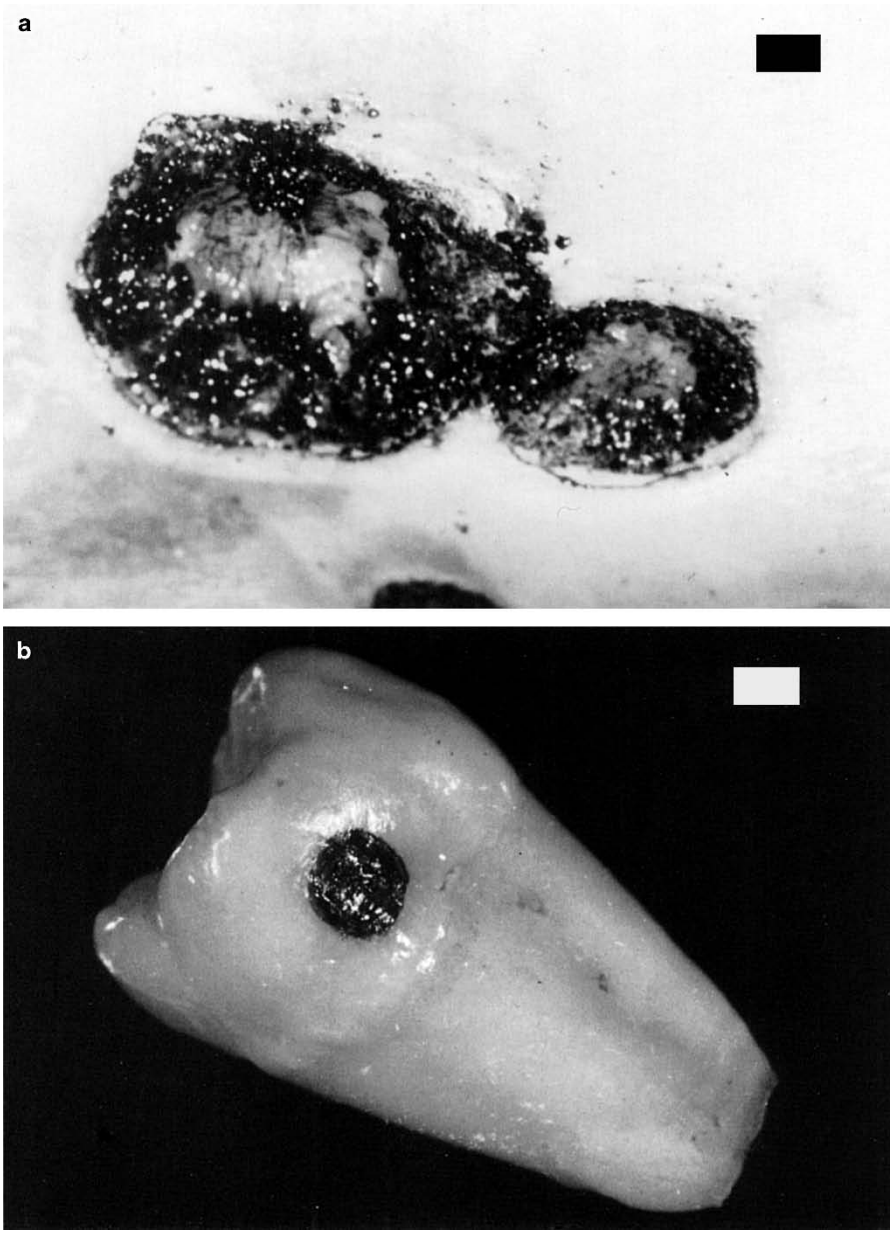

Fig. 3.12. (a) Tumor metastases on human skin carbonized with a CW CO_2 laser (power: 40 W, bar: 1 mm). Photograph kindly provided by Dr. Kurek (Heidelberg). **(b)** Human tooth carbonized with a CW CO_2 laser (power: 1 W, bar: 1 mm)

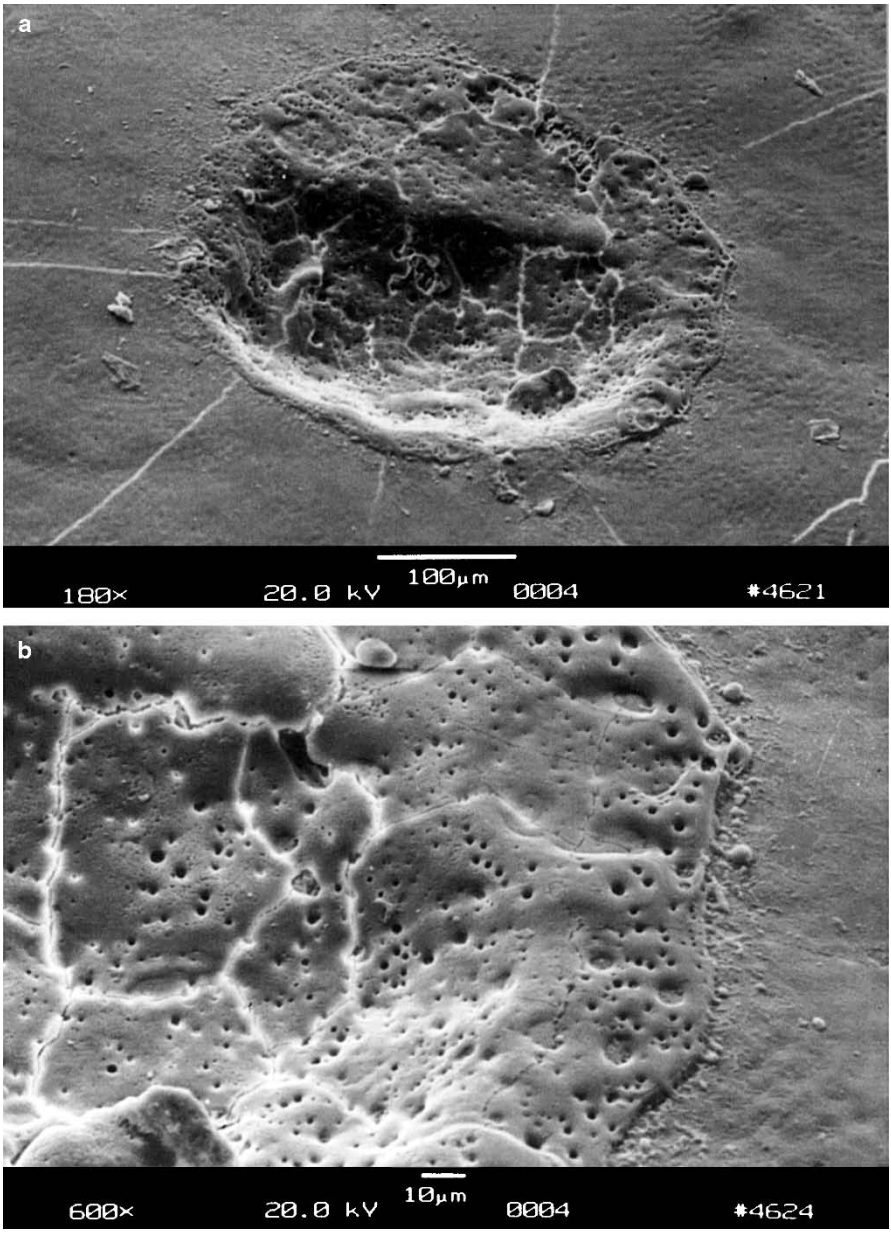

Fig. 3.13. (a) Human tooth melted with 100 pulses from a Ho:YAG laser (pulse duration: 3.8 µs, pulse energy: 18 mJ, repetition rate: 1 Hz). **(b)** Enlargement showing the edge of the melted zone

Temperature certainly is the governing parameter of all thermal laser–tissue interactions. And, for the purpose of predicting the thermal response, a model for the temperature distribution inside the tissue must be derived. Before we start working on this task, let us first look at the basics of what happens during thermal interaction.

At the microscopic level, thermal effects have their origin in bulk absorption occurring in molecular vibration–rotation bands followed by nonradiative decay. The reaction with a target molecule A can be considered as a two-step process. First, absorption of a photon with an energy $h\nu$ promotes the molecule to an excited state A^*; and second, inelastic collisions with some partner M of the surrounding medium lead to a deactivation of A^* and a simultaneous increase in the kinetic energy of M. Therefore, the temperature rise microscopically originates from the transfer of photon energy to kinetic energy. This two-step process can be written as

- absorption: $\mathrm{A} + h\nu \longrightarrow \mathrm{A}^*$,
- deactivation: $\mathrm{A}^* + \mathrm{M}(E_{\mathrm{kin}}) \longrightarrow \mathrm{A} + \mathrm{M}(E_{\mathrm{kin}} + \Delta E_{\mathrm{kin}})$.

How efficient is this two-step process? To answer this question, we have to consider both steps separately. First, absorption is facilitated due to the extremely large number of accessible vibrational states of most biomolecules. Second, the channels available for deactivation and thermal decay are also numerous, because typical energies of laser photons (Er:YAG laser: 0.35 eV, Nd:YAG laser: 1.2 eV, ArF laser: 6.4 eV) exceed by far the kinetic energy of a molecule at room temperature which is only about 0.025 eV. Thus, both of these steps are highly efficient provided the duration of laser exposure is properly selected.

The spatial extent and degree of tissue damage primarily depend on magnitude, exposure time, and placement of deposited heat inside the tissue. The deposition of laser energy, however, is not only a function of *laser parameters* such as wavelength, power density, exposure time, spot size, and repetition rate. It also strongly depends on *optical tissue properties* like absorption and scattering coefficients. For the description of storage and transfer of heat, *thermal tissue properties* are of primary importance such as heat capacity and thermal conductivity.

In biological tissue, absorption is mainly due to the presence of free water molecules, proteins, pigments, and other macromolecules as discussed in Sect. 2.3. It is governed by Lambert's law which we already encountered in (2.13). The absorption coefficient strongly depends on the wavelength of the incident laser radiation. In thermal interactions, absorption by water molecules plays a significant role. Therefore, the absorption spectrum of water – one important constituent of most tissues – is plotted in Fig. 3.14. In the visible range, the absorption coefficient of water is extremely small. In this section of the spectrum and in the UV, absorption in tissue is higher than shown in Fig. 3.14, depending on the relative content of macromolecules such as melanin and hemoglobin. Toward the IR range of the spectrum, however,

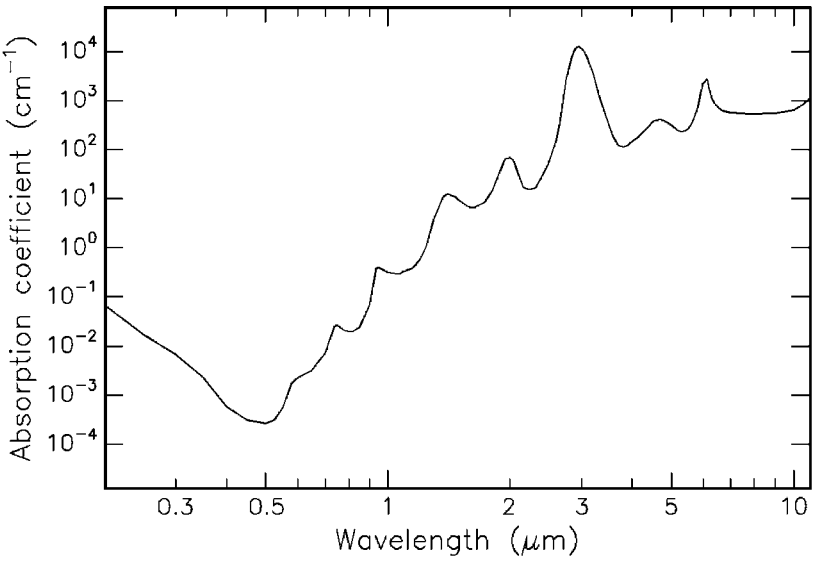

Fig. 3.14. Absorption of water. Data calculated from Hale and Querry (1973)

water molecules are the dominant absorbers, since their absorption coefficient then increases by several orders of magnitude. Typical absorption coefficients α and the corresponding absorption lengths L for the most important laser wavelengths are summarized in Table 3.3. It should be borne in mind that the total attenuation in the UV is strongly enhanced by Rayleigh scattering as discussed in Sect. 2.3.

Table 3.3. Absorption coefficients α and absorption lengths L of water at different wavelengths. Data calculated from Hale and Querry (1973)

Wavelength (nm)	Laser type	α (cm^{-1})	L (cm)
193	ArF	0.1	10
248	KrF	0.018	55
308	XeCl	0.0058	170
351	XeF	0.0023	430
514	Argon ion	0.00029	3400
633	He-Ne	0.0029	340
694	Ruby	0.0056	180
800	Diode	0.020	50
1053	Nd:YLF	0.57	1.7
1064	Nd:YAG	0.61	1.6
2120	Ho:YAG	36	0.028
2940	Er:YAG	12 000	0.00008
10600	CO_2	860	0.001

The absorption peak at about 3 μm – as shown in Fig. 3.14 – is of considerable interest. It originates from symmetric and asymmetric vibrational modes of water molecules as illustrated in Fig. 3.15. According to Pohl (1976), the resonance frequencies of these vibrational modes are 1.08×10^{14} Hz and 1.13×10^{14} Hz, respectively. These correspond to a wavelength close to 3 μm, thereby explaining the high absorption peak at this wavelength. Thus, the family of Er^{3+} doped lasers (Er:YAG at 2.94 μm, Er:YLF at 2.8 μm, and Er:YSGG at 2.79 μm) is a typical representative of thermally acting lasers. A similar argument applies for the wavelength of the Ho:YAG laser at 2.12 μm which also matches an absorption peak of water.

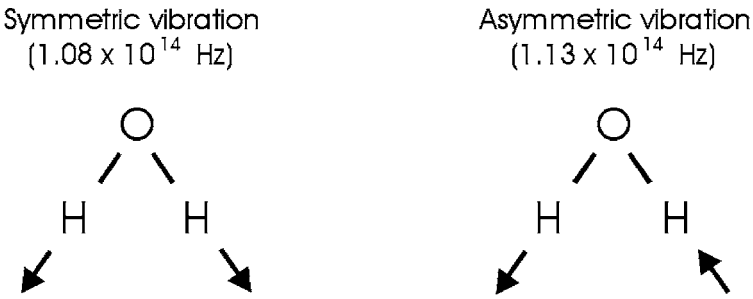

Fig. 3.15. Vibrational oscillations of water molecules

So far, we have encountered the basic origins of thermal effects, and we will now proceed to setting up a model explaining the basic physics involved. In order to derive a model which describes thermal effects quantitatively, several input parameters have to be taken into account. They are summarized in a flow chart as shown in Fig. 3.16.

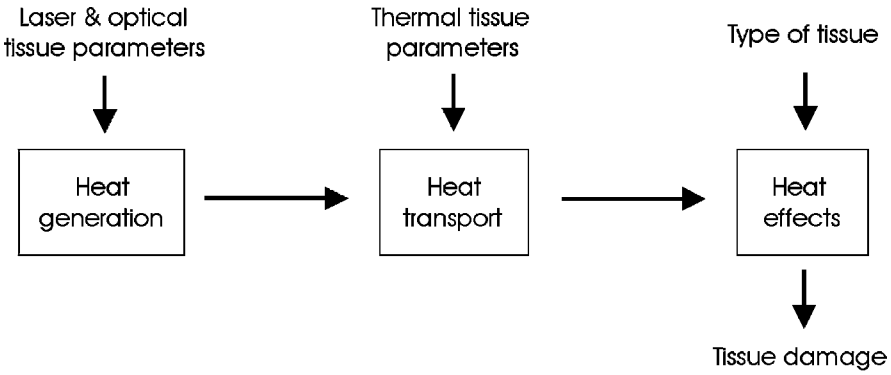

Fig. 3.16. Flow chart with important parameters for modeling thermal interaction

Heat generation is determined by laser parameters and optical tissue properties – primarily irradiance, exposure time, and the absorption coefficient – with the absorption coefficient itself being a function of the laser wavelength. *Heat transport* is solely characterized by thermal tissue properties such as heat conductivity and heat capacity. *Heat effects*, finally, depend on the type of tissue and the temperature achieved inside the tissue.

We assume that a slab of tissue is exposed in air to a Gaussian-shaped laser beam as illustrated in Fig. 3.17. For the sake of simplicity, a cylindrical geometry is chosen with z denoting the optical axis, and r the distance from this axis. Then, the amplitude of the electric field and the corresponding intensity inside the tissue are given by

$$\boldsymbol{E}(r,z,t) = \boldsymbol{E}_0 \exp\left(-\frac{r^2}{w^2} - \frac{\alpha z}{2}\right) \exp\left(-\frac{4t^2}{\tau^2}\right) , \tag{3.1}$$

$$I(r,z,t) = I_0 \exp\left(-\frac{2r^2}{w^2} - \alpha z\right) \exp\left(-\frac{8t^2}{\tau^2}\right) , \tag{3.2}$$

where $\boldsymbol{E}_0$ and I_0 are the incident values of electric field and intensity, respectively, w is the beam waist, α is the absorption coefficient, and τ is the pulse duration. From (3.2), we obtain that either at $r = w$ or at $t = \tau/2$ the intensity is cut down to $1/\mathrm{e}^2$ of its incident value. The incident values $\boldsymbol{E}_0$ and I_0 are related to each other by the basic electrodynamic equation

$$I_0 = \frac{1}{2}\,\varepsilon_0 c \boldsymbol{E}_0^2 ,$$

where ε_0 is the dielectric constant, and c is the speed of light. Scattering inside the tissue is neglected in a first approximation. Calculations taking scattering effects into account will be found at the end of this section.

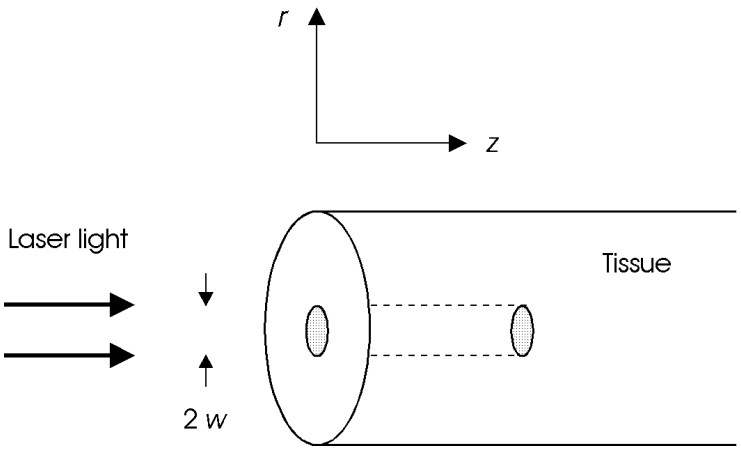

Fig. 3.17. Geometry of tissue irradiation

3.2.1 Heat Generation

By means of the two-step process as described above, heat is generated inside the tissue during laser exposure. Deposition of heat in tissue is due only to light that is absorbed in the tissue. For a light flux in the z-direction in a nonscattering medium, the local heat deposition per unit area and time in a thickness Δz is given by

$$S(r,z,t) = \frac{I(r,z,t) - I(r,z+\Delta z,t)}{\Delta z} \quad \text{in units of} \quad \frac{\mathrm{W}}{\mathrm{cm}^3} \ .$$

And, as Δz approaches zero,

$$S(r,z,t) = -\frac{\partial I(r,z,t)}{\partial z} \ .$$

Therefore, under all circumstances, heat deposition is determined by

$$S(r,z,t) = \alpha I(r,z,t) \ . \tag{3.3}$$

Thus, the heat source $S(r,z,t)$ inside the exposed tissue is a function of the absorption coefficient α and the local intensity $I(r,z,t)$. Since α is strongly wavelength-dependent, the same applies for S. If phase transitions (vaporization, melting) or tissue alterations (coagulation, carbonization) do not occur, an alteration in heat content $\mathrm{d}Q$ induces a linear change in temperature $\mathrm{d}T$ according to a basic law of thermodynamics

$$\mathrm{d}Q = m\,c\,\mathrm{d}T \ , \tag{3.4}$$

where m is the tissue mass, and c is the specific heat capacity expressed in units of kJ kg^{-1} K^{-1}. According to Takata et al. (1977), for most tissues, a good approximation is given by

$$c = \left(1.55 + 2.8\ \frac{\varrho_{\mathrm{w}}}{\varrho}\right)\ \frac{\mathrm{kJ}}{\mathrm{kg\ K}} \ ,$$

where ϱ is the tissue density expressed in units of kg/m^3, and ϱ_{w} is its water content expressed in units of kg/m^3. In the case of water, i.e. $\varrho_{\mathrm{w}} = \varrho$, the last relation reduces to

$$c = 4.35\ \frac{\mathrm{kJ}}{\mathrm{kg\ K}} \quad \text{at} \quad T = 37^{\circ}\mathrm{C} \ .$$

3.2.2 Heat Transport

Within a closed physical system, the relationship between temperature and heat content is described by (3.4). In real laser–tissue interactions, however, there are losses of heat to be taken into account, as well. They are based on either *heat conduction*, *heat convection*, or *heat radiation*. Usually, the latter two can be neglected for most types of laser applications. One typical example

of heat convection in tissue is heat transfer due to blood flow. The perfusion rates of some human organs are summarized in Table 3.4. Due to the low perfusivity of most tissues, however, heat convection is negligible in a first approximation. Only during long exposures and in special cases such as laser-induced interstitial thermotherapy (LITT) does it play a significant role and should be considered by adding a negative heat loss S_{loss} to the source term S. Heat radiation is described by the *Stefan–Boltzmann law* which states that the radiated power is related to the fourth power of temperature. Due to the moderate temperatures achieved in most laser–tissue interactions, heat radiation can thus often be neglected.

Table 3.4. Blood perfusion rates of some selected human organs. Data according to Svaasand (1985)

Tissue	Perfusion rate (ml $\text{min}^{-1}\,\text{g}^{-1}$)
Fat	0.012 – 0.015
Muscle	0.02 – 0.07
Skin	0.15 – 0.5
Brain	0.46 – 1.0
Kidney	$\simeq$ 3.4
Thyroid gland	$\simeq$ 4.0

Heat conduction, though, is a considerable heat loss term and is the primary mechanism by which heat is transferred to unexposed tissue structures. The heat flow $\boldsymbol{j}_Q$ is proportional to the temperature gradient according to the general diffusion equation[2]

$$\boldsymbol{j}_Q = -k\ \nabla T\ . \tag{3.5}$$

Herein, the constant k is called *heat conductivity* and is expressed in units of $\text{W m}^{-1}\ \text{K}^{-1}$. According to Takata et al. (1977), k can be approximated by

$$k = \left(0.06 + 0.57\ \frac{\varrho_{\text{w}}}{\varrho}\right)\ \frac{\text{W}}{\text{m K}}\ .$$

In the case of water, i.e. $\varrho_{\text{w}} = \varrho$, the last relation reduces to

$$k = 0.63\ \frac{\text{W}}{\text{m K}} \quad \text{at} \quad T = 37^{\circ}\text{C}\ .$$

The dynamics of the temperature behavior of a certain tissue type can also be expressed by a combination of the two parameters k and c. It is called *temperature conductivity* and is defined by

[2] This equation is the analog to the electrodynamic equation $\boldsymbol{j} = -\sigma\ \nabla\phi$, where $\boldsymbol{j}$ is the electric current density, σ is the electric conductivity, and ϕ is the electric potential.

$$\kappa = \frac{k}{\varrho c} \quad \text{in units of} \quad \frac{\mathrm{m}^2}{\mathrm{s}} \ . \tag{3.6}$$

The value of κ is approximately the same for liquid water and most tissues – about $1.4 \times 10^{-7}\,\mathrm{m}^2/\mathrm{s}$ according to Boulnois (1986) – since a decrease in heat conductivity due to a lower water content is usually compensated by a parallel decrease in heat capacity.

With these mathematical prerequesites, we are able to derive the general heat conduction equation. Our starting point is the *equation of continuity* which states that the temporal change in heat content per unit volume[3], $\dot{q}$, is determined by the divergence of the heat flow $\boldsymbol{j}_Q$:

$$\mathrm{div}\ \boldsymbol{j}_Q = -\,\dot{q}\ . \tag{3.7}$$

Inserting (3.7) into (3.4) leads to

$$\dot{T} = \frac{1}{mc}\,\dot{Q} = \frac{1}{\varrho c}\,\frac{\dot{Q}}{V} = \frac{1}{\varrho c}\,\dot{q} = -\,\frac{1}{\varrho c}\,\mathrm{div}\ \boldsymbol{j}_Q\ . \tag{3.8}$$

The other important basic equation is the diffusion equation, i.e. (3.5). Its combination with (3.8) yields

$$\dot{T} = \kappa\ \Delta T\ , \tag{3.9}$$

where Δ is the *Laplace operator*. This is the homogeneous *heat conduction equation* with the temperature conductivity as defined by (3.6). With an additional heat source S like the absorption of laser radiation, (3.8) and (3.9) turn into the inhomogeneous equations

$$\dot{T} = -\,\frac{1}{\varrho c}\,(\mathrm{div}\ \boldsymbol{j}_Q - S)\ , \tag{3.10}$$

$$\dot{T} = \kappa\ \Delta T + \frac{1}{\varrho c}\,S\ . \tag{3.11}$$

Next, we want to solve the homogeneous part of the heat conduction equation, i.e. (3.9). It describes the decrease in temperature after laser exposure due to heat diffusion. In cylindrical coordinates, (3.9) can be expressed by

$$\dot{T} = \kappa\ \left(\frac{\partial^2}{\partial r^2} + \frac{1}{r}\,\frac{\partial}{\partial r} + \frac{\partial^2}{\partial z^2}\right)\ T\ , \tag{3.12}$$

with the general solution

$$T(r,z,t) = T_0 + \frac{\chi_0}{(4\pi\kappa t)^{3/2}}\ \exp\left(-\,\frac{r^2+z^2}{4\kappa t}\right)\ , \tag{3.13}$$

[3] Note that q in (3.7) is expressed in units of $\mathrm{J/cm}^3$, while Q is in units of J. We thus obtain according to *Gauss' theorem*: $\int \mathrm{d}V\,\mathrm{div}\,\boldsymbol{j}_Q = \oint \mathrm{d}f\,\boldsymbol{j}_Q = -\,\dot{Q}$.

where T_0 is the initial temperature, and χ_0 is an integration constant. The proof is straightforward. We simply assume that (3.13) represents a correct solution to (3.12) and find

$$\dot{T} = -\frac{3}{2}\frac{T-T_0}{t} + \frac{r^2+z^2}{4\kappa t^2}\ (T-T_0)\ ,$$

$$\frac{\partial^2}{\partial r^2}T = \frac{\partial}{\partial r}\left(-2r\frac{T-T_0}{4\kappa t}\right) = -\frac{T-T_0}{2\kappa t} + 4r^2\frac{T-T_0}{16\kappa^2 t^2}\ ,$$

$$\frac{1}{r}\frac{\partial}{\partial r}T = -\frac{T-T_0}{2\kappa t}\ ,$$

$$\frac{\partial^2}{\partial z^2}T = \frac{\partial}{\partial z}\left(-2z\frac{T-T_0}{4\kappa t}\right) = -\frac{T-T_0}{2\kappa t} + 4z^2\frac{T-T_0}{16\kappa^2 t^2}\ .$$

Hence,

$$\kappa\ \Delta T = -\frac{T-T_0}{2t} + r^2\frac{T-T_0}{4\kappa t^2} - \frac{T-T_0}{2t} - \frac{T-T_0}{2t} + z^2\frac{T-T_0}{4\kappa t^2}\ ,$$

$$\kappa\ \Delta T = -\frac{3}{2}\frac{T-T_0}{t} + \frac{r^2+z^2}{4\kappa t^2}\ (T-T_0) = \dot{T} \quad \text{, q.e.d.}$$

The solution to the inhomogeneous heat conduction equation, (3.11) strongly depends on the temporal and spatial dependences of $S(r,z,t)$. Usually, it is numerically evaluated assuming appropriate initial value and boundary conditions. Nevertheless, an analytical solution can be derived if the heat source function $S(r,z,t)$ is approximated by a delta-function

$$S(r,z,t) = S_0\ \delta(r-r_0)\ \delta(z-z_0)\ \delta(t-t_0)\ .$$

For the sake of simplicity, we assume that the heat conduction parameters are isotropic[4]. Thus,

$$S(z,t) = S_0\ \delta(z-z_0)\ \delta(t-t_0)\ .$$

In this case, the solution can be expressed by a one-dimensional *Green's function* which is given by

$$G(z-z_0, t-t_0) = \frac{1}{\sqrt{4\pi\kappa(t-t_0)}}\ \exp\left[-\frac{(z-z_0)^2}{4\kappa(t-t_0)}\right]\ . \tag{3.14}$$

By means of this function, the general solution for a spatially and temporally changing irradiation is determined by

$$T(z,t) = \frac{1}{\varrho c}\int_0^t \int_{-\infty}^{+\infty} S(z',t')\ G(z-z',t-t')\ \mathrm{d}z'\ \mathrm{d}t'\ . \tag{3.15}$$

[4] A valuable theoretical approach to the three-dimensional and time-dependent problem is found in the paper by Halldorsson and Langerholc (1978).

The spatial extent of heat transfer is described by the time-dependent *thermal penetration depth*

$$z_{\text{therm}}(t) = \sqrt{4\kappa t} \ . \tag{3.16}$$

The term "penetration depth" originates from the argument of the exponential function in (3.14), since (3.16) turns into

$$\frac{z^2_{\text{therm}}(t)}{4\kappa t} = 1 \ .$$

Thus, $z_{\text{therm}}(t)$ is the distance in which the temperature has decreased to 1/e of its peak value. In Table 3.5, the relationship expressed by (3.16) is evaluated for water ($\kappa = 1.4 \times 10^{-7}\,\text{m}^2/\text{s}$). We keep in mind that heat diffuses in water to approximately 0.7 µm within 1 µs.

Table 3.5. Thermal penetration depths of water

Time t	Thermal penetration depth $z_{\text{therm}}(t)$
1 µs	0.7 µm
10 µs	2.2 µm
100 µs	7 µm
1 ms	22 µm
10 ms	70 µm
100 ms	0.22 mm
1 s	0.7 mm

For thermal decomposition of tissues, it is important to adjust the duration of the laser pulse in order to minimize thermal damage to adjacent structures. By this means, the least possible necrosis is obtained. The scaling parameter for this time-dependent problem is the so-called *thermal relaxation time* according to Hayes and Wolbarsht (1968) and Wolbarsht (1971). It is obtained by equating the optical penetration depth L as defined by (2.16) to the thermal penetration depth z_{therm}, hence

$$L = \sqrt{4\kappa\tau_{\text{therm}}} \ , \tag{3.17}$$

where τ_{therm} is the thermal relaxation time. One might argue the significance of τ_{therm}, because it is a theoretically constructed parameter. During thermal decomposition, however, τ_{therm} becomes very important, since it measures the thermal susceptibility of the tissue. This shall be explained by the following consideration: for laser pulse durations $\tau < \tau_{\text{therm}}$, heat does not even diffuse to the distance given by the optical penetration depth L. Hence, thermal damage of nondecomposed tissue is neglible. For $\tau > \tau_{\text{therm}}$, heat can diffuse to a multiple of the optical penetration depth, i.e. thermal damage of tissue adjacent to the decomposed volume is possible.

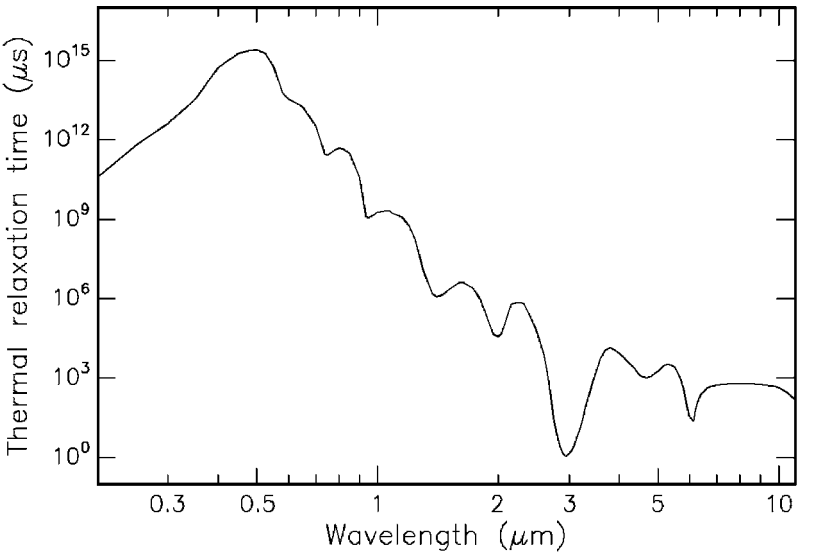

Fig. 3.18. Thermal relaxation times of water

Because of (3.17), the wavelength-dependence of L^2 is transferred to τ_{therm}. In Fig. 3.18, thermal relaxation times of water are shown as calculated from Fig. 3.14 and (3.17). We find that the shortest thermal relaxation time of approximately 1 µs occurs at the absorption peak of water near 3 µm. We may thus conclude that laser pulse durations $\tau < 1$ µs are usually[5] not associated with thermal damage. This statement is also referred to as the "1 µs rule".

– *Case I:* $\tau < 1$ µs. For nano- or picosecond pulses, heat diffusion during the laser pulse is negligible. If, in addition, we make the simplifying assumption that the intensity is constant during the laser pulse, we obtain from (3.3) that

$$S = \alpha I_0 \ .$$

For a quantitative relationship $T(t)$ at the tissue surface ($r = z = 0$), we may write

$$T = \left\{ \begin{array}{ll} T_0 + \frac{\alpha I_0}{\varrho c}\ t & \text{for } 0 \le t \le \tau \\ T_0 + T_{\max}\left(\frac{\tau}{t}\right)^{3/2} & \text{for } t > \tau \end{array} \right\} \ , \tag{3.18}$$

where $T_{\max}$ is the maximum increase in temperature given by

$$T_{\max} = \frac{\alpha I_0}{\varrho c}\ \tau \quad \text{at} \quad t = \tau \ .$$

[5] Laser pulses shorter than 1 µs can also lead to thermal effects if they are applied at a high repetition rate as discussed later in this section.

In Fig. 3.19, the temporal evolution of temperature in the pigment epithelium of the retina is shown according to (3.18). By neglecting heat diffusion during the short laser pulse, the temperature first increases linearly with respect to time. After the laser pulse, i.e. $t > \tau$, it decreases according to $t^{-3/2}$ as determined by the solution to the homogeneous heat conduction equation. The thermally damaged zone is shorter than the optical absorption length. Thus, thermal damage to adjacent tissue can be kept small if a wavelength is selected that is strongly absorbed by the tissue. In the case of tissues with a high water content, Er:YAG and Er:YSGG lasers are potential candidates for this task. However, only a few groups like Andreeva et al. (1986), Eichler et al. (1992), and Pelz et al. (1994) have reported on mode locking of these lasers. But their operation is not yet stable enough for clinical applications. Alternatives might soon arise due to recent advances in the development of tunable IR lasers such as the optical parametric oscillator (OPO) and the free electron laser (FEL).

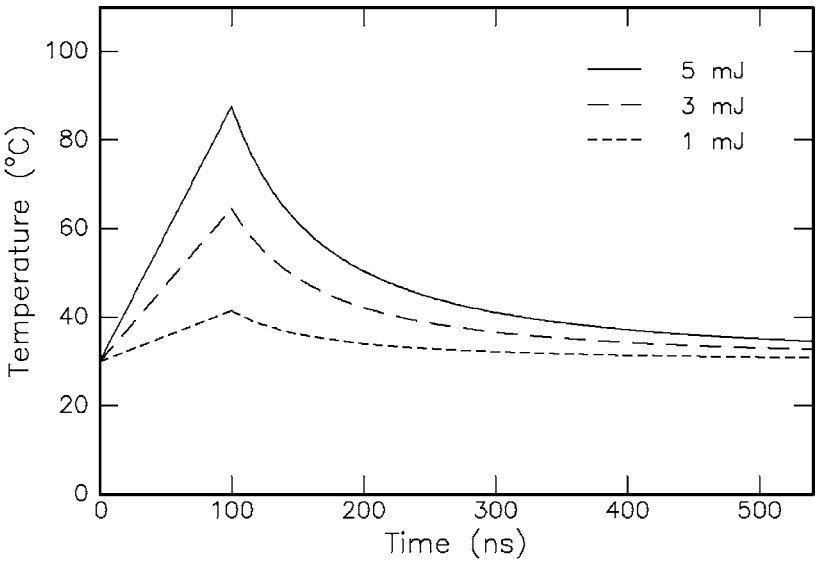

Fig. 3.19. Temporal evolution of temperature in the pigment epithelium of the retina during and after exposure to a short laser pulse ($\tau = 100\,\text{ns}$, beam diameter: 2 mm, pulse energy: as labeled, $T_0 = 30^\circ\text{C}$, $\alpha = 1587\,\text{cm}^{-1}$, $\varrho = 1.35\,\text{g cm}^{-3}$, and $c = 2.55\,\text{J g}^{-1}\,\text{K}^{-1}$). Tissue parameters according to Hayes and Wolbarsht (1968) and Weinberg et al. (1984)

– *Case II:* $\tau > 1\,\mu\text{s}$. For pulse durations during which heat diffusion is considerable, the thermally damaged zone is significantly broadened. In this case, the solution to the inhomogeneous heat conduction equation cannot be given analytically but must be derived numerically, for instance by using the methods of *finite differences* and *recursion algorithms*. This procedure

becomes necessary because heat diffusion during the laser pulse can no longer be neglected. Thus, for this period of time, temperature does not linearly increase as assumed in (3.18) and Fig. 3.19. Detailed simulations were performed by Weinberg et al. (1984) and Roggan and Müller (1993). One example is found in Fig. 3.24 during the discussion of laser-induced interstitial thermotherapy.

A high repetition rate ν_{rep} of the laser pulses can evoke an additional increase in temperature if the rate of heat transport is less than the rate of heat generation. The dependence of temperature on repetition rate of the laser pulses was modeled by van Gemert and Welch (1989). The significance of the repetition rate becomes evident when looking at Figs. 3.20a–b. In this case, 1000 pulses from a picosecond Nd:YLF laser were focused on the same spot of a human tooth at a repetition rate of 1 kHz. Although, usually such short pulses do not evoke any thermal effect as discussed above, radial cracking and melting obviously occurred at the surface of the tooth. In particular, the enlargement shown in Fig. 3.20b demonstrates that the chemical compounds of the tooth had melted and recrystallized in a cubic structure. Thus, the temperature achieved must have reached a few hundred °C due to insufficient heat transport.

In order to get a basic feeling for typical laser parameters, the following very simple calculations might be very useful. We assume that a pulse energy of 3 µJ is absorbed within a tissue volume of 1000 μm^3 which contains 80 % water. The amount of water in the specified volume is equal to $8\times10^{-10}\,\text{cm}^{-3}$ or 8×10^{-10} g, respectively. There are now three steps to be taken into account when aiming for a rough approximation of the final temperature. First, energy is needed to heat the tissue up to 100°C. Second, energy is transferred to vaporization heat. And third, the remaining energy leads to a further increase in temperature of the water vapor.

– Step 1: 37°C $\longrightarrow$ 100°C (assumed body temperature: 37°C)

$$Q_1 = mc\Delta T = 8\times10^{-10}\,\text{g}\;4.3\,\frac{\text{kJ}}{\text{kg}\;^\circ\text{C}}\;63^\circ\text{C} = 2.2\times10^{-7}\,\text{J}.$$

– Step 2: Vaporization at 100°C

$$Q_2 = mQ_{\text{vap}} = 8\times10^{-10}\,\text{g}\;2253\,\frac{\text{kJ}}{\text{kg}} = 1.8\times10^{-6}\,\text{J}.$$

– Step 3: 100°C $\longrightarrow T_{\text{fin}}$

$$Q_3 = 3\,\mu\text{J} - Q_1 - Q_2 = 0.98\,\mu\text{J},$$

$$T_{\text{fin}} = 100^\circ\text{C} + \frac{Q_3}{mc} = 100^\circ\text{C} + \frac{0.98\,\mu\text{J}}{8\times10^{-10}\,\text{g}\;4.3\,\text{kJ}\,(\text{kg}\,^\circ\text{C})^{-1}} \simeq 385^\circ\text{C}.$$

Thus, the resulting temperature is approximately 385°C.

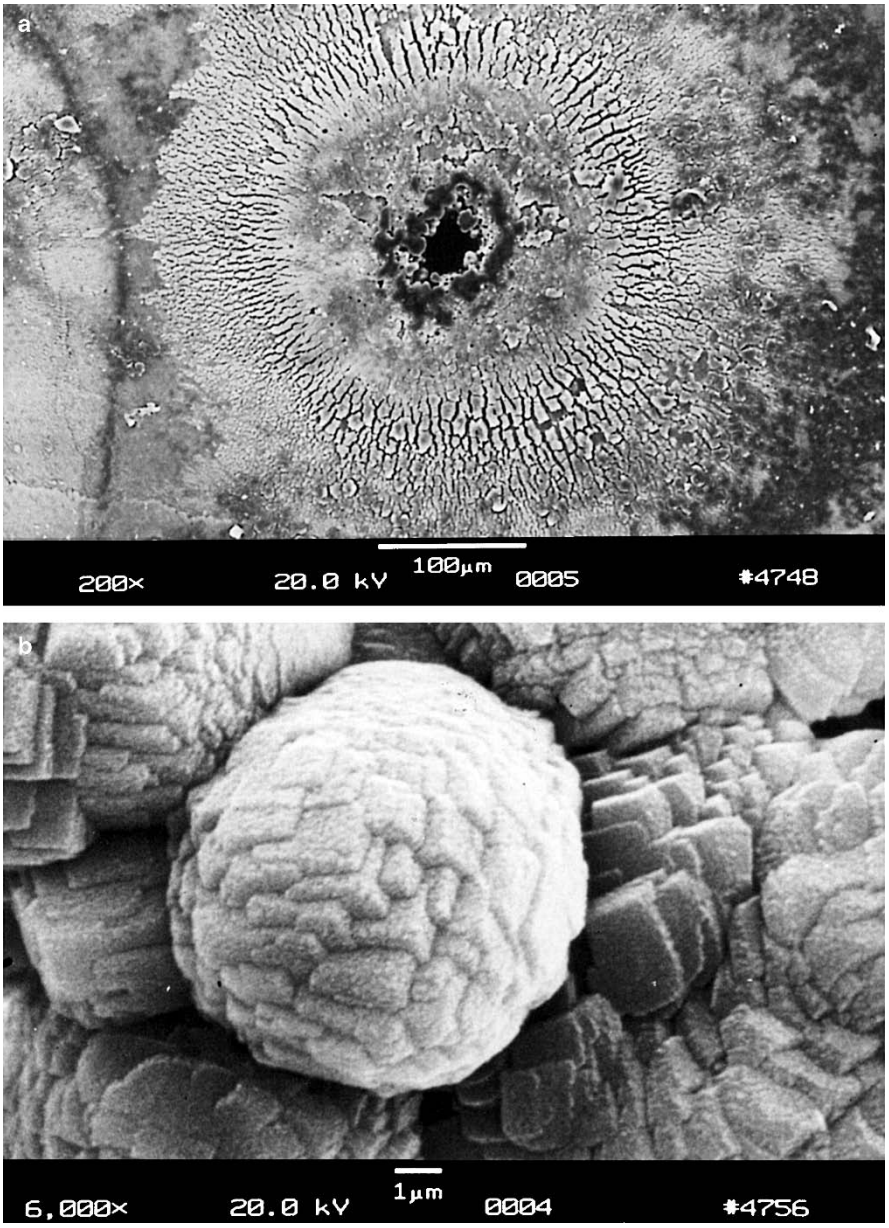

Fig. 3.20. (a) Hole in tooth created by focusing 1000 pulses from a Nd:YLF laser on the same spot (pulse duration: 30 ps, pulse energy: 1 mJ, repetition rate: 1 kHz). **(b)** Enlargement showing cubic recrystallization in form of plasma sublimations. Reproduced from Niemz (1994a).

3.2.3 Heat Effects

The model developed above usually predicts the spatial and temporal distribution of temperature inside tissue very well if an appropriate initial value and boundary conditions are chosen. This, however, is not always an easy task. In general, though, approximate values of achievable temperatures can often be estimated. Therefore, the last topic in our model of thermal interaction deals with biological effects related to different temperatures inside the tissue. As already stated at the beginning of this section, these can be manifold, depending on the type of tissue and laser parameters chosen. The most important and significant tissue alterations will be reviewed here.

Assuming a body temperature of 37°C, no measurable effects are observed for the next 5°C above this. The first mechanism by which tissue is thermally affected can be attributed to conformational changes of molecules. These effects, accompanied by bond destruction and membrane alterations, are summarized in the single term *hyperthermia* ranging from approximately 42–50°C. If such a hyperthermia lasts for several minutes, a significant percentage of the tissue will already undergo necrosis as described below by *Arrhenius' equation*. Beyond 50°C, a measurable reduction in enzyme activity is observed, resulting in reduced energy transfer within the cell and immobility of the cell. Furthermore, certain repair mechanisms of the cell are disabled. Thereby, the fraction of surviving cells is further reduced.

At 60°C, denaturation of proteins and collagen occurs which leads to coagulation of tissue and necrosis of cells. The corresponding macroscopic response is visible paling of the tissue. Several treatment techniques such as laser-induced interstitial thermotherapy (LITT) aim at temperatures just above 60°C. At even higher temperatures (> 80°C), the membrane permeability is drastically increased, thereby destroying the otherwise maintained equilibrium of chemical concentrations.

At 100°C, water molecules contained in most tissues start to vaporize. The large vaporization heat of water (2253 kJ/kg) is advantageous, since the vapor generated carries away excess heat and helps to prevent any further increase in the temperature of adjacent tissue. Due to the large increase in volume during this phase transition, gas bubbles are formed inducing mechanical ruptures and thermal decomposition of tissue fragments.

Only if all water molecules have been vaporized, and laser exposure is still continuing, does the increase in temperature proceed. At temperatures exceeding 100°C, carbonization takes place which is observable by the blackening of adjacent tissue and the escape of smoke. To avoid carbonization, the tissue is usually cooled with either water or gas. Finally, beyond 300°C, melting can occur, depending on the target material.

All these steps are summarized in Table 3.6, where the local temperature and the associated tissue effects are listed. For illustrating photographs, the reader is referred to Figs. 3.10–3.13 and Fig. 3.20.

Table 3.6. Thermal effects of laser radiation

Temperature	Biological effect
37°C	Normal
45°C	Hyperthermia
50°C	Reduction in enzyme activity, cell immobility
60°C	Denaturation of proteins and collagen, coagulation
80°C	Permeabilization of membranes
100°C	Vaporization, thermal decomposition (ablation)
> 100°C	Carbonization
> 300°C	Melting

In general, the exact temperature for the onset of cell necrosis is rather difficult to determine. As a matter of fact, it was observed that not only the temperature achieved but also the temporal duration of this temperature plays a significant role for the induction of irreversible damage. It is illustrated in Fig. 3.21 how the critical temperature and the corresponding temporal duration relate to each other if irreversible damage is meant to occur. The curve is derived from several empirical observations. In the example selected in Fig. 3.21, a temperature of 60°C lasting for at least 6 s will lead to irreversible damage.

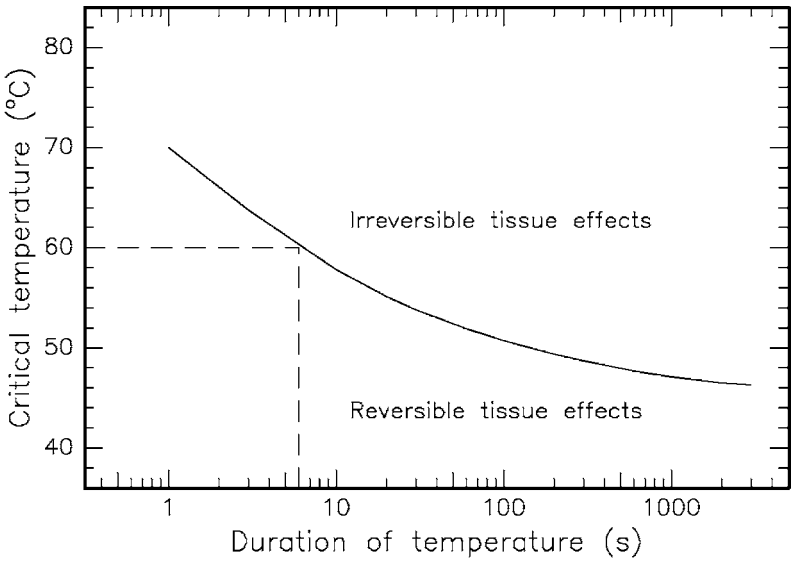

Fig. 3.21. Critical temperatures for the occurrence of cell necrosis. Data according to Henriques (1947) and Eichler and Seiler (1991)

Areas in which the temperature reaches values higher than 60°C are coagulated, and irradiated tissue cells become necrotic. Areas with maximum temperatures less than 60°C are treated hyperthermically only, and the probability of cells staying alive depends on the duration and temporal evolution of the temperature obtained. For a quantitative approximation of the remaining active molecules and cells at a certain temperature level, *Arrhenius' equation* is very useful:

$$\ln \frac{C(t)}{C_0} = -A \int_0^t \exp\left(-\frac{\Delta E}{RT(t')}\right) \mathrm{d}t' \equiv -\Omega \ , \tag{3.19}$$

where C_0 is the initial concentration of molecules or cells, $C(t)$ is the concentration at a time t, A is Arrhenius' constant, R is the universal gas constant, and ΔE and Ω are specific tissue properties. According to Welch (1984), the coefficient A can be approximated by

$$A \simeq \frac{kT}{h} \exp \frac{\Delta S}{R} \ ,$$

where ΔS is the activation entropy, k is Boltzmann's constant, and h is Planck's constant. But, according to Johnson et al. (1974), this relation has no simple significance.

The local degree of tissue damage is determined by the damage integral given in (3.19). The damage degree is defined as the fraction of deactivated molecules or cells given by

$$D_\mathrm{d}(t) = \frac{C_0 - C(t)}{C_0} = 1 - \exp\left(-\Omega\right) \ .$$

Thus, by inserting an appropriate value of the tissue constant Ω, we are able to calculate the probable damage degree $D_\mathrm{d}(t)$ as a function of time t. This was performed by Weinberg et al. (1984) in the case of retinal tissue.

Unfortunately, experimental data for the two parameters A and ΔE are very difficult to obtain due to the inhomogeneity of most tissues and the uncertainty in measuring the surviving fraction. However, in Table 3.7 some values of various tissues are listed as found in different studies.

Table 3.7. Arrhenius' constants of different tissues

Tissue	$A(s^{-1})$	ΔE (J/mol)	Reference
Retina	1.0×10^{44}	2.9×10^5	Vassiliadis et al. (1971) Weinberg et al. (1984)
Retina ($T < 50°\mathrm{C}$)	4.3×10^{64}	4.2×10^5	Takata et al. (1977)
Retina ($T > 50°\mathrm{C}$)	9.3×10^{104}	6.7×10^5	Takata et al. (1977)
Skin	3.1×10^{98}	6.3×10^5	Henriques (1947)
Liver	1.0×10^{70}	4.0×10^5	Roggan and Müller (1993)

Laser radiation acts thermally if power densities $\geq 10\,\mathrm{W/cm^2}$ are applied from either CW radiation or pulse durations exceeding approximately 1 µs. Typical lasers for coagulation are Nd:YAG lasers or diode lasers. CO_2 lasers are very suitable for vaporization and the precise thermal cutting of tissue. Carbonization and melting can occur with almost any type of laser if sufficient power densities and exposure durations are provided.

Frequently, not only one but several thermal effects are induced in biological tissue, depending on the laser parameters. These effects might even range from carbonization at the tissue surface to hyperthermia a few millimeters inside the tissue. In most applications, though, only one specific effect is aimed at. Therefore, careful evaluation of the required laser parameters is essential. Reversible and irreversible tissue damage can be distinguished. Carbonization, vaporization, and coagulation certainly are irreversible processes, because they induce irrepairable damage. Hyperthermia, though, can turn out to be either a reversible or an irreversible process, depending on the type of tissue and laser parameters. Since the critical temperature for cell necrosis is determined by the exposure time as shown in Fig. 3.21, no well-defined temperature can be declared which distinguishes reversible from irreversible effects. Thus, exposure energy, exposure volume, and exposure duration together determine the degree and extent of tissue damage. The coincidence of several thermal processes is illustrated in Fig. 3.22. The location and spatial extent of each thermal effect depend on the locally achieved temperature during and after laser exposure.

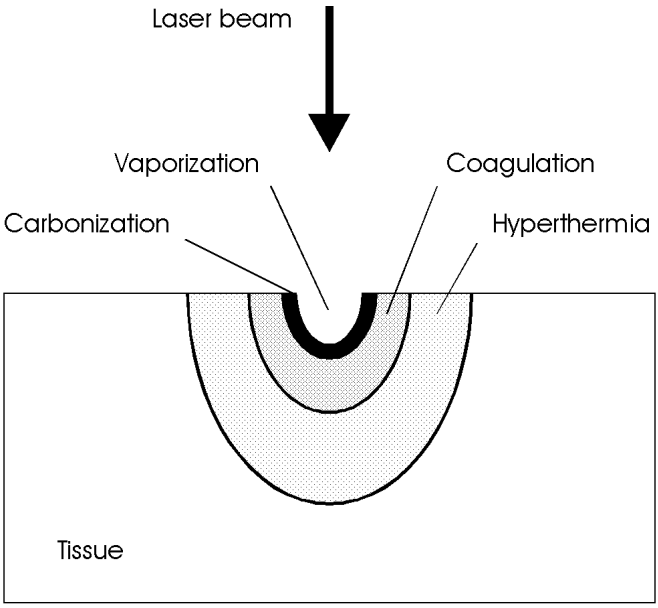

Fig. 3.22. Location of thermal effects inside biological tissue